Jurnal
Teknologi

Full Paper

AXIAL DEFORMATION OF SPINE BIO-TENSEGRITY MODEL AT DIFFERENT DEPLOYABLE SCHEMES

Nur Hazira Rosli[a], Syed Muhammad Syed Yahya[b]*, Lee Siong Wee[b], Toku Nishimura[c], Oh Chai Lian[d]

[a]China Communication Construction (ECRL) Sdn Bhd, Section 8, Ecosky, 188, Jln Kuching, Taman Tasik Indah, 51200 Kuala Lumpur, Malaysia
[b]School of Civil Engineering, College of Engineering, Universiti Teknologi MARA, 81750, Masai, Johor, Malaysia
[c]Department of Architecture, College of Architecture, Kanazawa Institute of Technology, Hakusan 924-0838, Japan
[d]School of Civil Engineering, College of Engineering, Universiti Teknologi MARA, 40450, Shah Alam, Selangor, Malaysia

Article history
Received
22 August 2023
Received in revised form
6 December 2024
Accepted
7 January 2024
Published Online
17 October 2024

*Corresponding author
syed9490@uitm.edu.my

Graphical abstract

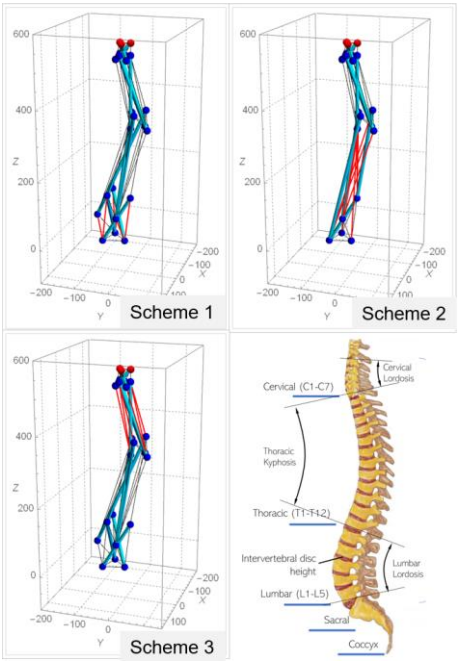

Abstract

The study presents the axial deformation of a spine bio-tensegrity model through a shape change strategy with different deployment schemes. The spine bio-tensegrity model mimics a human spine's total height, tapered form and natural curvature. Three deployable schemes S1-S3 with a different combination of cables at alterable and fixed lengths were investigated to achieve a series of axial displacements at 200 mm, 400 mm and 600 mm in the z-direction. The shape change algorithm was developed to optimise the forced elongation of cables, incorporating an objective function designed for monitored nodes in the system to reach their prescribed targets during the optimisation process. Sequential quadratic programming was employed to solve a nonlinear optimisation problem involving inequality constraints in the shape change analysis. The efficiency of the deployable systems was assessed based on the deformed shapes, convergence curve, and axial forces of the spine bio-tensegrity model. The finding shows that in addition to axial deformation, the model S1 deployment scheme preserves the slenderness characteristic of the spine. In contrast, the model exhibits excessive expansion in the thoracic region in schemes S2 and S3. Greater total computational steps in deployment scheme S3, followed by S2 and S1, reveal that the active cables set near the monitored nodes allow the model to sense and act faster to reach their targets. The study contributes to understanding the structural behavior and deployment strategy for a structure mimicking a biological system and it can be extended to applications such as deployable structures and biomechanical studies.

Keywords: Bio-tensegrity, convergence curve, deployable, sequential quadratic programming, spine

Abstrak

Kajian ini membentangkan pengubahsuaian paksi model bio-tensegriti tulang belakang melalui strategi perubahan bentuk dengan pelbagai skema penyebaran. Model bio-tensegrity tulang belakang menyerupai ketinggian

keseluruhan tulang belakang manusia, bentuk dan kelengkungan semulajadi. Tiga skema yang boleh dikerahkan S1-S3 dengan kombinasi kabel yang berbeza pada panjang yang boleh diubah dan tetap telah disiasat untuk mencapai satu siri pergeseran paksi pada 200 mm, 400 mm dan 600 mm dalam arah z. Algoritma perubahan bentuk telah dibangunkan untuk mengoptimumkan pemanjangan paksa kabel, dengan memasukkan fungsi objektif yang direka untuk nod yang dipantau dalam sistem agar mencapai sasaran yang ditetapkan semasa proses pengoptimuman. Pengaturcaraan kuadratik berurutan digunakan untuk menyelesaikan masalah pengoptimuman bukan linear yang melibatkan sekatan ketaksamaan dalam analisis perubahan bentuk. Kecekapan sistem yang boleh dikerahkan dinilai berdasarkan bentuk yang terdeformasi, lengkung penumpuan, dan daya paksi model bio-tensegriti tulang belakang. Penemuan ini menunjukkan bahawa selain daripada deformasi paksi, skema pelaksanaan model S1 mengekalkan ciri kekemasan tulang belakang. Sebaliknya, model tersebut menunjukkan pengembangan yang berlebihan di kawasan toraks dalam skema S2 dan S3. Jumlah langkah pengiraan yang lebih besar dalam skema penyebaran S3, diikuti oleh S2 dan S1, menunjukkan bahawa set kabel aktif yang diletakkan berhampiran nod yang dipantau membolehkan model untuk merasai dan bertindak dengan lebih pantas untuk mencapai sasaran mereka. Kajian ini menyumbang kepada pemahaman tingkah laku struktur dan strategi penyebaran untuk struktur yang meniru sistem biologi dan ia boleh diperluaskan kepada aplikasi seperti struktur yang boleh dikerahkan dan kajian biomekanik.

Kata kunci: Bio-tensegriti, lengkung penumpuan, pergerakan, pengaturcaraan kuadratik berurutan, tulang belakang

1.0 INTRODUCTION

Tensegrity principle lays with isolated compression surrounded with continuous tension. Combination of compressive (i.e. bars/struts) and tensile components (i.e. strings/cables) create a stable network and efficient load paths for tensegrity system, distributing applied loads internally within the system. Tensegrity owns favorable characteristics such as high efficiency, strong stiffness, adjustability, impressive strength to weight ratio and outstanding environment adaptability [5]. The beneficial features of tensegrity resulted in various types of technology and applies in many areas of art, architecture, civil engineering, biomedical structural model, mechanical metamaterials, and currently in flexible robotics [1; 2; 5; 10; 17; 20].

Tensegrity is a self-equilibrated spatial reticulated structure. The structure can stand freely without external load due to the pre-stresses present within its members. Tensegrity had been analysed into a special class at a border between mechanism and structure. When the member lengths and orientations change, tensegrity remains equilibrium and stable, although it has deformed over large displacement. This principle leads to the potential of deployable structures that are with force equilibrium throughout the deployment. Tensegrity was introduced as a deployable structure in the 1990s, and tensegrity robots since the 2000s owing to the characteristics as mentioned earlier. Recent works were reviewed in [9].

On the one hand, the principle of bio-tensegrity integrates the principle of tensegrity with biological systems. The bio-tensegrity principle explains the anatomy and physiology of human orgsnisms such as spine, elbows, muscles, skins, mechanotransduction, body movement, etc. The application of the principle of bio-tensegrity at the macro to the nanoscale of the biology systems is supported with overwhelming evidence [7; 15]. For example, the bio-tensegrity concept of having tension and compression members can be seen in the compressive passive subsystem (i.e., spinal column) and tensional active subsystem (i.e., muscles and tendons) in the human skeletal system. In addition, the biological structure is a unique structure that has the characteristic of mobility, flexible hinged, low energy consuming, omnidirectional structures that act in a gravity-free environment as indicated in the tensegrity principle [8]. The bio-tensegrities in the human body exhibit nonlinear visco-elastic properties throughout the movement. The principle of tensegrity in the human body system is recognised with all the components in the system supported with structural stability in every movement, and ligaments work to limit the motion [14]. The studies of biotensegrity model is also suggested for future investigations to predict important results in future investigations of "long COVID-19" particularly based on the model of

myofibroblast-generated-tensegrity-tension and extracellular matrix alterations [13]. A combination of biology and tensegrity in robotics in the construction industry to reduce human dependency especially involving high-risk tasks is also recommended [10].

There are many studies on shape change strategies of tensegrity structures. [18] employed an open-loop control technique to compute the deployment of tensegrities, and generated the reference trajectories by second-order functions to avoid rapid accelerations and decelerations. A nonlinear finite element analysis was then used to study the dynamic characteristics in deploying foldable tensegrity-membrane systems. [21] investigated the quasi-static deployment of tensegrities with member length actuation and subjected to load-carrying stiffness constraints. The relationship between the driving elongation of members and the load-induced displacement during the deployment was established. [19] developed general methods to analyse the deployment of Class-1 and Class-2 tensegrity booms. The deployment strategy involves a few considerations such as relationships between the circumscribing circle's height, twist angle, and radius. [16] proposed a general optimisation-based approach for the design of minimal mass active tensegrity structures based on a mixed integer programming scheme. The typical design of the active tensegrities significantly show a decrement of the material consumption compared with the equivalent passive designs. [20] designed a collision resilient aerial vehicle tensegrity structures with a proposed controller that can make rotation tasks easier. However, limited studies were reported on the shape change of bio-tensegrity. [11] proposed a shape change method to analyse the deployment of spine bio-tensegrity models with the introduction of forced elongation in cables. The deployment method considers all cables are active and can alter their length for the model to achieve the targets via bending, axial and torsional deformation, which may be costly in the design. Thus, this paper proposes three deployment schemes that reduce some active cables at different locations for a spine bio-tensegrity model. The efficiency of the various deployable schemes was evaluated based on the deformed shapes, convergence curve and axial forces of the spine bio-tensegrity model.

This paper is structured as follows: Section 2 explains the methodology of the study such as the configurations of the spine bio-tensegrity model, the shape change method and the deployment schemes. Section 3 presents the discusses the effectiveness of the proposed deployable schemes via numerical examples of spine biotensegrity model. Lastly, conclusions are presented in Section 4.

2.0 METHODOLOGY

This section explains the methodology of the shape change analysis and the deployable schemes in the computational of the axial deformations of a spine bio-tensegrity model. The geometrical and material properties of the spine bio-tensegrity model was adopted from the author's previous study [4]. The bio-tensegrity model was chosen to investigate the mechanical properties of the tensegrity model mimicking the human spine in performing exaggerated extension. This study is motivated with the ability of human spine in adapting multi-directional movement and stable although there is self-structural reorganisation.

2.1 Spine Bio-tensegrity Model: Geometrical & Material Properties

Spine bio-tensegrity model adopted from [4] was generated based on geometrical input data from anatomical parameters of human spines obtained from [3]. The geometrical input data was based on human spine specimens from six male cadavers with age and body height ranges from 55-84 years old and 174-192 cm, respectively. The anatomy parameters of the human spine were considered in the study, particularly the dimensions of the vertebrae (Figure 1a) and the natural sagittal curvature (Figure 1b). Natural sagittal curvature of the human spine consists of two main angles: cervical and lumbar lordosis and thoracic kyphosis. The development of the curvature of spine bio-tensegrity model was based on the C7 plump line located at the end of lordosis at the cervical region. The width of the spine vertebrae (EPW) and heights of the vertebrae (VBHC) and intervertebral disc (IDH) were obtained for the establishment of the model configuration.

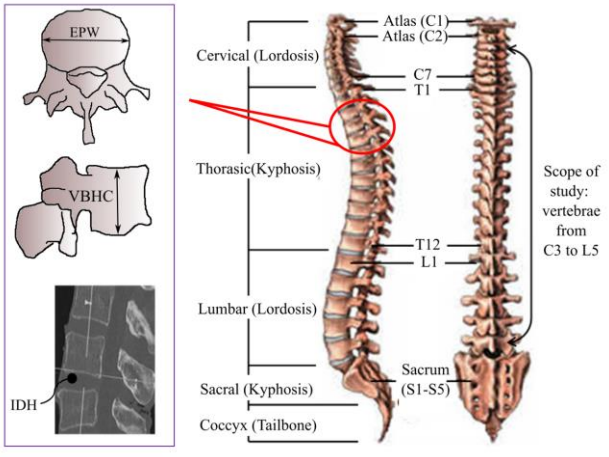

(a) (b)

Figure 1 (a) Vertebrae Anatomical Parameters (b) Natural Sagittal Curvature [13]; (Oh *et al.*, 2020)

Figure 2 shows the spine bio-tensegrity model with the set-up of a combination of struts and cables. The struts in the bio-tensegrity model represent spine vertebrae which are connected by cables that represent human muscles. The model is classified as Class 1 tensegrity model. There is no contact between struts, mimicking human spine vertebrae that are separated from the intervertebral disc. The model consists of a total of sixty-nine (69) elements with twelve (12) struts and fifty-seven (57) cables. The struts are indicated in blue cylinders, while the cables are in thin black lines. There is a stacked up of four (4) basic cells based on three-strut tensegrity (i.e. simplex) configuration forming the spine bio-tensegrity model. The details of nodal coordinates, elemental connectivity and establishment processes of the bio-tensegroty model mimicking human spine were presented in [4].

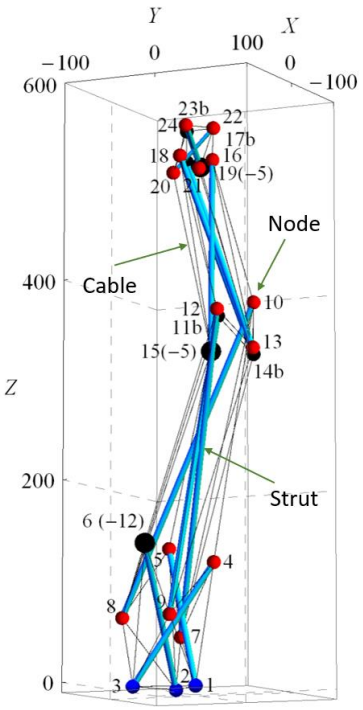

Figure 2 Self-equilibrated configuration for spine bio-tensegrity model (Oh *et al*., 2020)

The spine bio-tensegrity is in the self-equilibrated and stable form under rest. A form-finding method based on equilibrium formulations of pin jointed bio-tensegrity model solved by Moore-Penrose generalised inverse can be found in [4].

2.2 Shape Change Method

The shape change method is summarised in Figure 3. Algorithm 1 shows the primary shape change analysis, whereas Algorithm 2, which is embedded in Algorithm 1 searches for the optimised forced elongation. Detail description on the shape change method can be found in [11; 12].

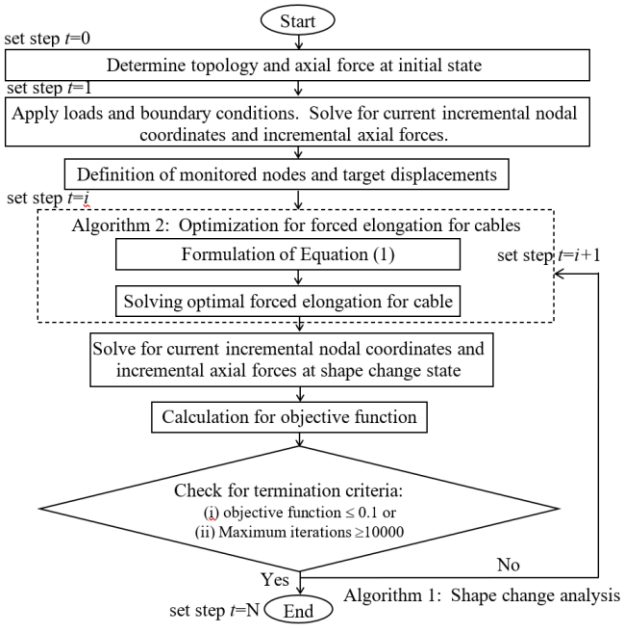

Figure 3 Shape change algorithm [11]

The first step of the shape change analysis is to prepare the geometrical information for the bio-tensegrity model. In this initial analysis state, step *t* is set as *t*=0. The bio-tensegrity's topology such as nodal coordinates and element connectivity were provided at this point. It is important to note that the bio-tensegrity must attain the self-stress in all elements in order to proceed to the next step. The axial forces were calculated by using the equilibrium equation *Bn*=0. The solution requires generalised inverse method in computing the linearly independent self-equilibrium stress mode and vectors. A potential combination of coefficients of linearly independent self-equilibrium vectors was determined considering allowable axial force in cable and struts.

Next, the inputs for deformed state of bio-tensegrity were prepared at the step *t*=1. External loads and boundary conditions were applied to the bio-tensegrity model in this deformed state. Self-weight is applied to all nodes in the model in this study. The three nodes forming the triangular surface at the base are fixed supported. When the bio-tensegrity model was loaded, the nodal coordinates and axial forces were updated. At this step, all the struts and cables undergo elastic deformations.

Next, monitored nodes and target coordinates were specified. Set *t*=2 as the first step in shape change state. The specification of monitored nodes and target coordinates is crucial for Algorithm 2 in the optimisation of forced elongation. One or more nodes can be defined as monitored nodes in the shape change analysis. The displacements of the nodes were then monitored if they were to reach the prescribed target coordinates. In this study, the top three nodes, nodes 22, 23 and 24 of the spine bio-tensegrity model were chosen as monitored nodes.

Once the monitored nodes and target coordinates were defined, Algorithm 2 ran to optimise the forced elongation of cables at every incremental steps. Only cables are allowed for a change in length or forced elongation in the shape change analysis. This is to mimic the shortening or extension of human muscles to deploy a human spine. In Algorithm 2, the sequential quadratic programming (SQP) method is used to solve the nonlinear optimisation problem. The forced elongation of a cable is calculated by solving the quadratic programming sub-problem with inequality constraints as expressed in Equation 1:

$$\min_{x \in R^n} f(\boldsymbol{x}) = \boldsymbol{g}^T {}^t\boldsymbol{l} + \frac{1}{2} {}^t\boldsymbol{l}^{\mathrm{T}} \boldsymbol{H} {}^t\boldsymbol{l} \quad \text{Eqn (1)}$$

$$\text{subject to } \boldsymbol{A}_2 {}^t\boldsymbol{l} \geq \boldsymbol{b}_2$$

where $\boldsymbol{g}$ is vector of distance between monitored node and target whereas ${}^t\boldsymbol{l}$ is vector of incremental forced elongation which corresponds to the optimisation variable and $\boldsymbol{H}$ is a positive-definite approximation of Hessian matrix of the Lagrangian function. Matrix $\boldsymbol{A}_2$ and vector $\boldsymbol{b}_2$ are the inequality constraints corresponding to the limitation in allowable axial forces and forced elongation, respectively. In order to ensure the stability of biotensegrity model, tangent stiffness matrix is checked for its positive definiteness in the computation.

The optimised forced elongation of cables is then used to calculate the incremental nodal coordinates and axial forces at every incremental step *t=i*.

Further to step 6 where the objective function is calculated as follows:

$$\min f(\boldsymbol{x}) = \left| {}^t\boldsymbol{x} - {}^f\boldsymbol{x} \right| \quad \text{Eqn. (2)}$$

where ${}^f\boldsymbol{x}$ is prescribed target coordinates, and ${}^t\boldsymbol{x}$'is the current coordinates, for all the specified monitored nodes at current step *t* during the shape change analysis.

Finally, the satisfaction of termination criteria is checked. The analysis of Algorithm 1 is checked for compliance with the termination criteria of (i) objective function in Eqn. 2 smaller than 0.1 or (ii) maximum iteration is greater than 10000. If the analysis meets either one of these criteria, Algorithm 1 will be terminated. Alternatively, the shape change analysis proceeds with step *t= i*+1 where the optimisation of a new set of forced elongation and subsequent processes are repeated until the termination criteria are met.

2.3 Deployment Schemes

Controlling all the cables for deployment is always costly and deals with complex computation. Thus, three deployment schemes proposed in this study employs only parts of the active cables instead of all cables in performing shape change. In addition to elastic elongation, the active cables are allowed to have additional elongation termed as forced elongation. This study investigates three deployment schemes which are differentiated with multiple combinations of active and undeformed cables. It is to note that the undeformed elements (i.e. passive cables) can only perform elastic elongation and not subjected to forced elongation. Specifically, each scheme indicates different cable groups, such as diagonal cables L1, L2 and L3 in the spine bio-tensegrity model that were set as undeformed elements. The cables that connect both ends to the base supports in the spine bio-tensegrity model are also undeformed elements. Table 1 shows the diagonal cable groups and the cables in the bio-tensegrity model according to its schemes that were chosen as undeformed elements. Figure 4 illustrates the undeformed elements in red for schemes S1, S2 and S3. There are six (6) undeformed cables in S1 and nine (9) undeformed cables in S2 and S3. Particularly, the diagonal cable group L1, L2 and L3 in the associated schemes S1, S2 and S3 are located at the lower, middle and upper part of the model, respectively. The diagonal cable group L4 is located at the cervical region and was not selected as undeformed elements due to the direct connection to the monitored nodes. These schemes were later evaluated for their effectiveness in the deployment and compared with the study in [12]; Oh *et al*., (2022) which utilises all the cables' lengths are alterable.

Table 1 Undeformed elements and deployment schemes

Scheme	Diagonal Cable Group	Numbers of Cable	Undeformed Elements (Cables)
S1	L1	6	37,38,39,40,41,42
S2	L2	9	43,44,45,46,47,48,49,50,51
S3	L3	9	52,53,54,55,56,57,58,59,60

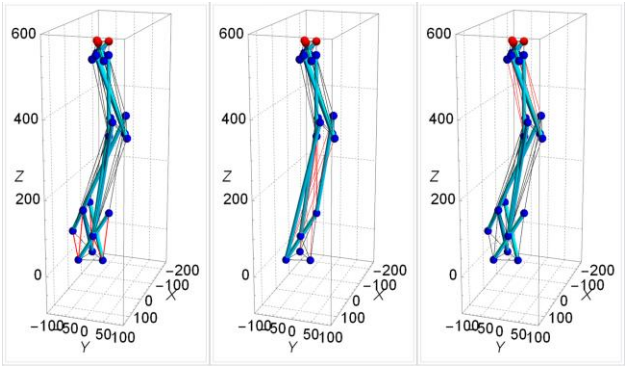

(a) (b) (c)

Figure 4 Undeformed elements (indicated in red elements) for (a) Scheme 1 (b) Scheme 2 (c) Scheme 3

The top three nodes (nodes 22, 23, and 24) in the bio-tensegrity model were assigned as monitored nodes that continually measured the displacement from the original coordinates to the target coordinates. Table 2 summarises the shape change analysis cases. The study explores the viability of

implementing a bio-tensegrity model to achieve extension beyond its initial height, ensuring the capability to reach at least its own height. Therefore, three analysis cases under each of the schemes for the model were carried out to advance to three different target coordinates, which are 200 mm, 400 mm and 600 mm in the z-direction away from the original coordinates of the monitored nodes. The target coordinates were prescribed in the z-direction to evaluate the potential of the bio-tensegrity model for axial deformation. The mechanical behaviour, such as the deformed shape and axial forces, were also evaluated under these schemes.

Table 2 Shape change analysis cases

Scheme	Series		
	z=200 mm	z=400 mm	z=600 mm
S1	S1Z200	S1Z400	S1Z600
S2	S2Z200	S2Z400	S2Z600
S3	S3Z200	S3Z400	S3Z600

3.0 RESULTS AND DISCUSSION

3.1 Axial Deformation of Bio-Tensegrity Model

This section discusses the deformed shape during the incremental shape change analysis and the final form of the spine bio-tensegrity model when reaching the targets. Shape changes or movement of the model from its initial state (at rest) until it reaches its final state are described. The final shape of the model for each scheme when it reaches the targeted coordinate is also presented.

3.1.1 Shape Changes of Bio-tensegrity Model

Figure 5 to Figure 7 show the shape change of the spine bio-tensegrity model for schemes S1 to S3 at series Z200, Z400 and Z600, respectively.

Shape Changes of Bio-tensegrity Model at Series Z200

The model deformed with a slight expansion at the thoracic region for scheme S1 at 25% of computational steps (*i*=33). At 50% of computational steps (*i*=67), the model keeps expanding at the same region while forced elongation at diagonal cable groups L3 and L4 towards the targets is clearly observed. The force elongations in cables have resulted in an upward displacement of around 100mm. At 75% of computational steps (*i*=100), the model behaves differently from earlier steps. Instead of expanding, it becomes slenderer as it squeezes the width and lengthens the body. Diagonal string L4 elongates towards the z-direction where the monitored nodes advanced from z=600 mm to z=700 mm. The model is straight without bending in any direction, as seen at the beginning of the deformation. While at the final deformation (*i*=133), when the monitored nodes achieved the targeted coordinate, the cervical region was slightly inclined to the positive y-axis.

For scheme S2, the model shows insignificant deformation at the early stage of shape change analysis (25% computational steps, *i* = 46). Obvious changes were observed at 50% of computational steps (*i*=93), when the width of the thoracic region increased. At 75% of computational steps (i=139) and final deformation (i=185) when it reaches target coordinates, the model demonstrates expansion at the thoracic region and contraction at the lower part of the cervical region of the model. The model overall shows axial deformation in the z direction in reaching the target coordinates without tilt.

The spine bio-tensegrity model in scheme S3 demonstrates an axial deformation to z-direction without tilt throughout the shape change analysis. The expansion in the thoracic region is observed. A few contributing nodes persistently displaced outward from the original position, resulting in the expansion of the model.

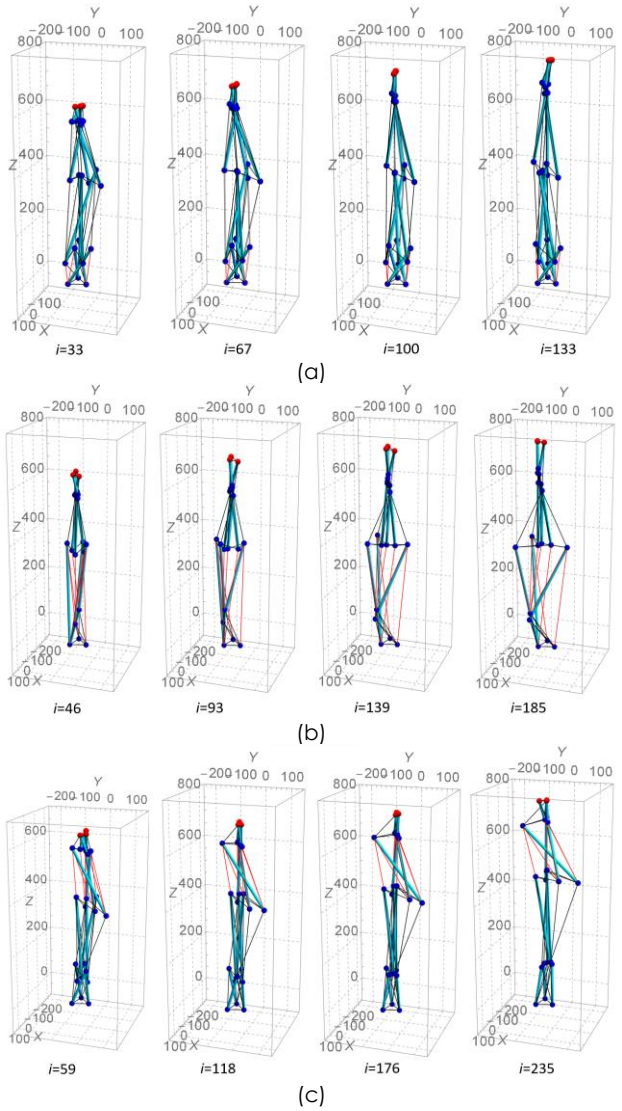

Figure 5 (a) Shape Changes of S1Z200 (b) Shape Changes of S2Z200 (c) Shape Changes of S3Z200

Shape Changes of Bio-tensegrity Model at Series Z400

For scheme S1 in series Z400, the model deformed in contraction and expansion throughout the shape change process. Most of the cables elongated to achieve the target coordinates. When the top three nodes almost reach the targets at step *i*=406, the cervical region expands slightly, and the model tends to tilt in a negative *y*-direction.

For scheme S2, the model displays an obvious deformation from step *i*=125. The model has shown obvious expansion at the lower part of the thoracic region. The width of the model gradually increased with the increment of the height after step *i*=250. In addition to axial deformation, when the top three nodes achieve their targeted coordinate, the model also shows a slight tilt to the positive y-axis.

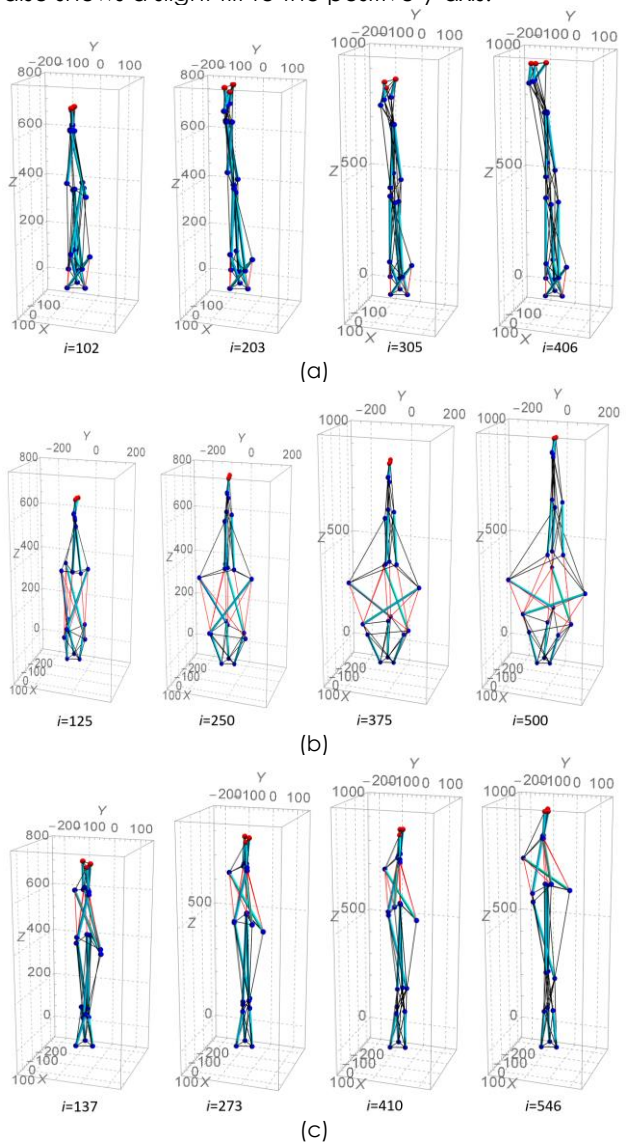

Figure 6 (a) Shape Changes for S1Z400 (b) Shape Changes for S2Z400 (c) Shape Changes for S3Z400

For scheme S3, the model slowly elongated from the original height to the targeted coordinate. The model also shows gradual expansion at the upper part of the thoracic region throughout the shape change analysis. At 75% of computational steps (*i*=410), the model tilted insignificantly in a negative *y*-direction.

Shape Changes of Bio-tensegrity Model at Series Z600

For scheme S1, the model started to expand at the thoracic region when some nodes were displaced apart from each other from 50% of computational steps (*i*=492). When the model reaches 75% of computational steps (*i*=738), the model starts to tilt at the negative y-axis. The model expanded with equal width at the thoracic region and extended axially in the z-direction to achieve the targets.

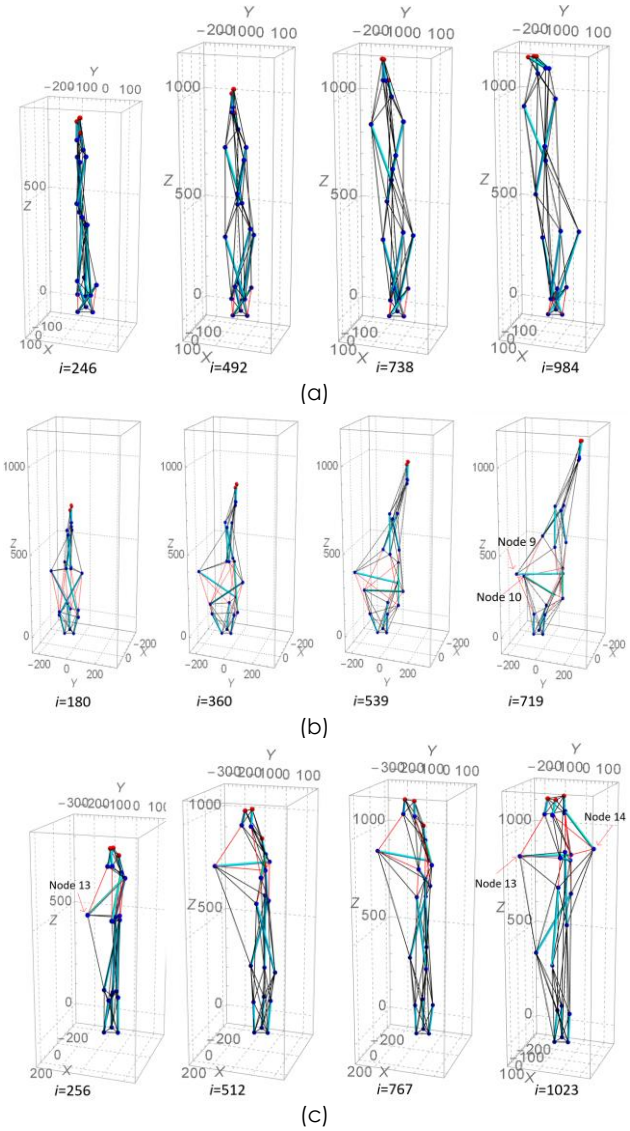

Figure 7 (a) Shape Changes for S1Z600 (b) Shape Changes for S2Z600 (c) Shape Changes for S3Z600

For scheme S2, the model behaved differently, where it slowly tilted to the positive y-axis starting from the early computational steps. At the same time, the model elongated to the z-direction. The lower part of the thoracic region expanded excessively while the top part of the region contracted. A few nodes (Node 9 and Node 10) noticeably drag back the model (towards a negative *y*-direction) to maintain the equilibrium and stability of the model.

For scheme S3, the deformed shape is almost the same for computational steps *i*=256 and *i*=767, in addition to a further extension towards the z-direction. There are two specific nodes, namely node 13 and node 14, which are displaced towards negative y and positive y, respectively, resulting in the obvious expansion of the cervical region.

3.1.2 Final Deformed Shape

Figure 8 shows the final deformed shape for the models at all schemes for series Z200, Z400 and Z600. The final deformed shape of the model scheme S1 for series Z200 almost exhibits the initial shape, which has a tapered form from the base to the top except for greater height. Meanwhile, in addition to axial deformation towards the z-direction, the final deformed shape for scheme S2 show an expansion at the lower part of the thoracic region and a shrinkage at the cervical region. Oppositely to scheme S2, the model in scheme S3 has an expanded part at the top part of the thoracic region at the final computation step.

In addition to a greater height as a result of achieving the targets at 400 mm in the z-direction from the initial coordinates, the models in all schemes behave quite similarly to series Z200. The model also presents greater width for series Z400 compared to Z200.

The models behave differently in series Z600 for all schemes. The final deformed shape for the model in scheme S1 has shown an increase in the overall width of the model. The model also demonstrates axial deformation in a straight (i.e. schemes S1 and S3) and inclined manner (i.e. scheme S2). Although the expansion is still observed in the lower part of the thoracic region for scheme 2, and the upper part of the thoracic region for scheme 3, displacements of a few specific nodes are noticeable. These nodes play roles in sustaining the self-equilibrated shape of the spine bio-tensegrity model in achieving the targets.

3.2 Computational Steps and Convergence Curves

Table 3 shows the total computational steps for all the analysis cases. The results are expected as higher computational steps are required for the model to achieve a greater targeted displacement. There are 2-3 times higher computational steps to achieve target displacements of 400 mm compared to 200 mm; and 3-7 times to achieve 600 mm compared to 200 mm.

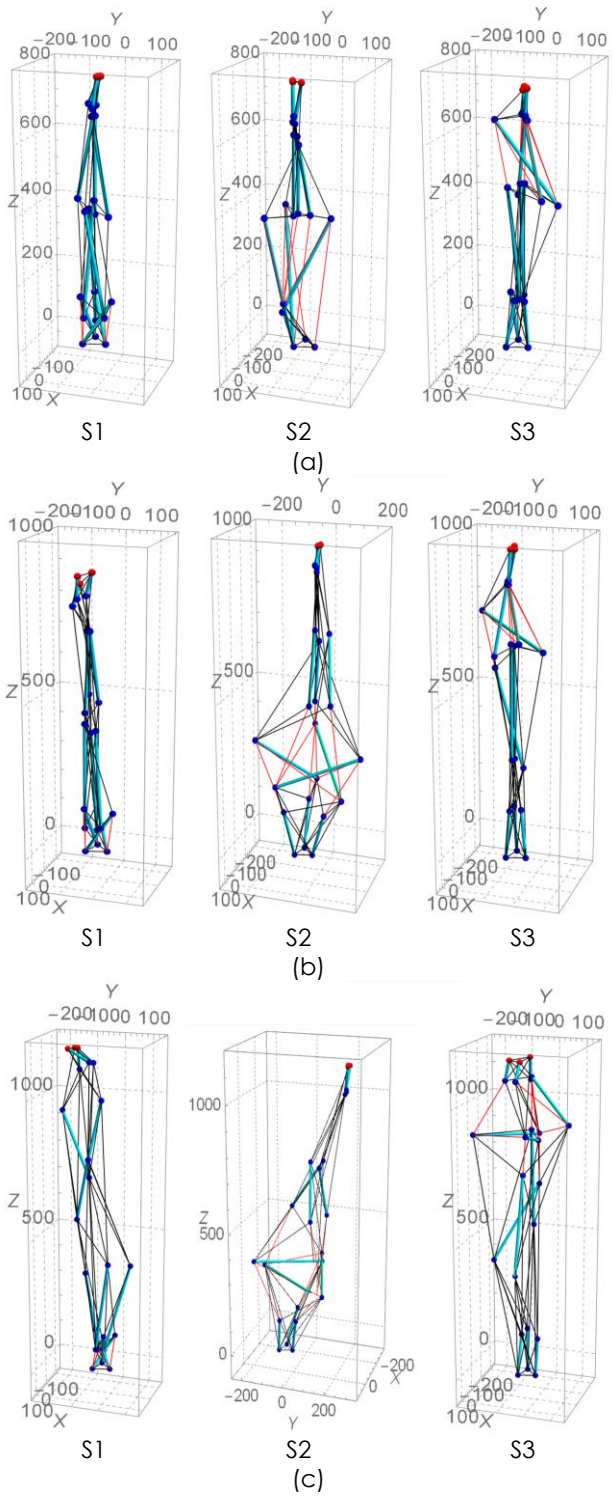

Figure 8 Final deformed shape of spine bio-tensegrity model (a) Series Z200 (b) Series Z400 (c) Series Z600

Most cases also demonstrate that schemes S2 and S3 require higher computational steps than Scheme 1.

Although the proposed schemes are relatively more economical, the computational time is greater than the model utilising forced deformation in all cables as in the Control model [11]. There is no limitation in lengths for all cables to perform large displacements, and all cables take part in optimising the objective function.

Table 3 Total computational steps

Scheme	Series			Z400/Z200	Z600/Z200
	Z200	Z400	Z600		
S1	133	406	984	3.1	7.4
S2	185	500	719	2.7	3.9
S3	235	546	1023	2.3	4.4
Control [11]	105	203	400	1.9	3.8

Figure 9 shows the convergence curves for all the shape change analysis cases. The convergence curve is the objective function value as a function of the computation step. The convergence curves are constructed from single searches until they reach the objective function or predefined maximum computational step. The efficiency of the deployment schemes for the model to achieve the targets is examined. In this study, all the analysis cases reach the objective function or the prescribed target coordinates instead of the predefined maximum computational step. The objective function for all the analysis cases was generalised with the normalised objective function (NOF), which was calculated based on the ratio of the objective function at the current step to the first step. All analysis cases show NOF=1 at the first step while NOF=0 when at the final step. The decrement of the NOF in the convergence curve at every incremental step also reveals the reduction in the distance between the monitored nodes and target coordinates.

It is found from Figure 9 that the convergence curves for all the analysis cases have shown two phases. In the first phase, the curves run linearly from the initial step. While in the second phase, the curves diverge from the linear line with a reduced slope. The divergence of the curves occurs more frequently and is obvious in the cases with higher target displacements in the shape change analysis.

For series Z200, the curves for all schemes show only a slight change in slope at NOF, approximately 0.45-0.55, with most of the time constructed in linear way. While for series Z400, the curves for all schemes show a more noticeable change in slope at NOF, approximately 0.75-0.85. Alternatively, the curve for scheme 2 runs differently with another obvious change in slope at NOF = 0.5. For series Z600, the curves for all schemes show an obvious change in slope at NOF, approximately 0.85. Curves for series 1 and 3 demonstrate another divergence at NOF of approximately 0.35. For all the series, at NOF of approximately 0.1, the curves typically took more computation steps to converge. The analysis case S1Z600 especially reached a plateau which took 105 out of 984 steps at NOF below 0.1 before converging.

The optimisation of the solutions through the iteration process has often affected the convergence solutions. The slowdown of the convergence reflected in a change of slope and subsequently reaching a plateau indicates that the algorithm settles into an optimum solution, which minimises the objective function. However, the configuration and placement of the undeformed elements of the spine biotensegrity model also contribute to the convergence of the solution. Two identified conditions possibly slow down the computational: (1) the struts (bones) and the undeformed cables (i.e. passive cables or non-active muscles) are unable to have additional elongation (i.e. forced elongation) and thus difficult to assist advancement to the target coordinates, and (2) restriction of having very small forced elongation each iteration to prevent large displacement in the algorithm.

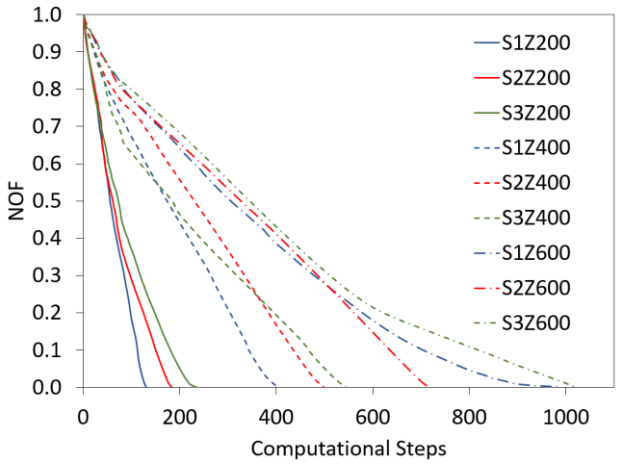

Figure 9 Convergence curve

3.3 Axial Forces

This section presents the axial forces of the spine biotensegrity model during the shape change. In the shape change process, all the elements satisfy the linear elastic material conditions and are kept within the material yield stress. The model is computed to maintain stability and equilibrium in forces throughout the computational step. In this study, the struts and cables must achieve compressive and tension forces, respectively, while the undeformed elements defined as bars can attain both forces. For elastic material properties, the lower and upper axial force limits for cables and bars are defined as:

$$0 \le n_c \le \sigma_c A_c \qquad \text{Eqn. (3)}$$

$$\max\left\{-\frac{\pi^2 E_s I_s}{l_s^2}, -\sigma_s A_s\right\} \le n_s \le \sigma_s A_s \qquad \text{Eqn (4)}$$

where n_c, σ_c and A_c are axial forces, yield stress and cross-sectional area for cable elements, respectively; n_s, E_s, I_s, L_s, σ_s and A_s are axial forces, Young modulus, moment of inertia, element length, yield stress and cross-sectional area for strut and bar elements, respectively. In this study, all strut elements have circular cross-section. Cables and struts are cross-sectional area of 3.14 mm^2 and 50.1 mm^2. The yield stress for all elements is 250 MPa. The lower limit of axial force for struts is -12567 N while the upper limit of axial force for cables is 785 N.

From the analysis results, it is found that all the analysis cases have satisfied the axial force constraints throughout the shape change analysis. Due to comprehensive data, analysis case S1Z200 is chosen to present the changes of axial forces for struts, cables and bar elements over the computational step, as shown in Figure 10.

Figure 10a shows the changes of axial forces for struts (i.e. elements 1-12) during the shape change. The axial forces of struts fluctuate from 0 N to -1549 N, which are within the axial force limits (i.e. -12567 N). Strut 8 remains at higher compression most of the time compared to other struts. Figure 10b shows the changes in axial forces for cables (i.e. elements 13-37 and 43-69). The axial forces of cables show more obvious fluctuation over the computational steps compared to struts. The cables are in tension and not exceeding the yield point (785 N). Most of the cables sustain axial forces that are lesser than 300 N. A few cables constantly reach high tension greater than 700 N for more than 50% of computational steps, particularly cables 20, 47, 65 and 25. Figure 10c shows the changes in axial forces for bars (i.e. elements 37-42). The bar elements show lesser fluctuation compared to cables. Some bar elements are constantly in compression and some in tension, while a few carry either compression or tension during the shape change analysis. Bar 41 shows exceptionally high axial force in the shape change analysis and requires further attention during the design.

3.4 Discussion

The spine bio-tensegrity presents axial deformation when the target displacements are prescribed at 200 mm to 600 mm in the positive z-direction. During the axial deformation in a shape change analysis, the increment of the target displacement increases the total computational steps. Most of the cables were lengthened by forced elongation to achieve the continual axial deformation, which indicates a direct relationship between the incremental forced elongation and target displacement. However, the increment of the total computational steps with the associated target displacements from 200 mm to 600 mm does not run linearly. The results are aligned with the convergence curves when the curves for cases with higher target displacements were constructed more nonlinear way. Longer computational steps required may be caused by the constraint of forced elongation, which is set very small (i.e. 0.5 mm) to ensure small deformation through the linear and static analysis. In addition, the restrictions in terms of the length of struts and undeformed elements can increase the incremental search in minimising the objective function.

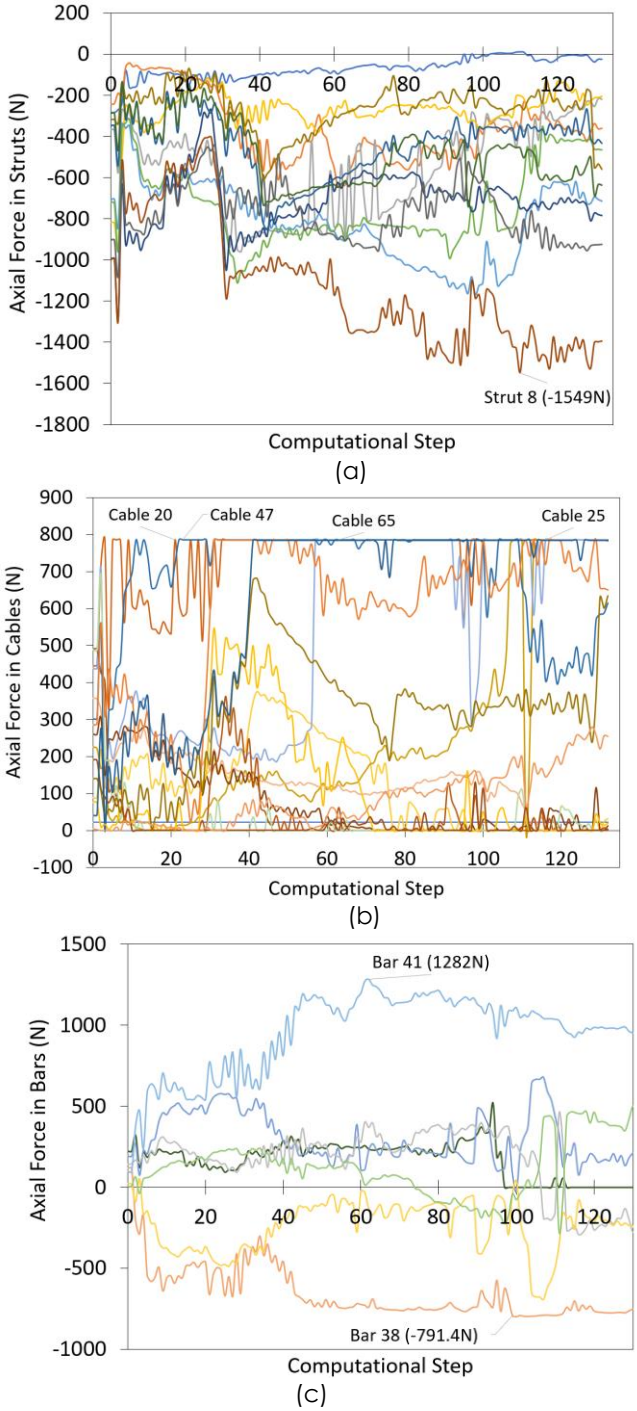

Figure 10 Axial Force for (a) Struts (b) Cables and (c) Bars of Analysis Case S1Z200

The deployment scheme S1 has better performance in terms of lesser total computational steps and has maintained the slenderness as the human spine during the shape change and at the final state. This can be explained based on the position of the undeformed elements, which the scheme S1, S2 and S3 are at lumbar, thoracic, and cervical regions, respectively. It is found that when the undeformed elements are located near to the monitored nodes (i.e. S2 and S3), excessive deformation in expansion were observed. The total computational steps for the model to reach the targets also increased. For scheme S1, the undeformed elements are located the farthest from the monitored nodes, allowing the activated cables which are surrounding the monitored nodes to respond faster (i.e. elongate) to achieve the targets. This finding has good agreement with actual neck motion, where the neck extension significantly associated with the increased muscle activation surrounded the neck, cervical and upper thoracic regions [6].

The axial forces of the model for all the analysis cases and deployable schemes are within the allowable forces. There are a few nodes and elements which play significant roles in maintaining the stability and equilibrium of the model during the shape change analysis. These nodes and elements shall be carefully monitored and designed for the shape change process.

4.0 CONCLUSIONS

This paper investigates the deformation of the spine bio-tensegrity model under different deployable schemes to reach 200 mm, 400 mm and 600 mm of target displacements. The topology of the model mimics the human spine's anatomy and natural curvature. The efficiency of three deployment schemes in the shape change performance of the spine bio-tensegrity was also evaluated.

The spine bio-tensegrity model undergoes axial deformation to achieve the target coordinates prescribed in the z-direction in all analysis cases. Acting like a cantilever system restrained at the base, the model displays straight and slight slanting to one side at the final state.

The model in deployment scheme S1 preserves the slenderness characteristic of the spine during the shape change analysis. Alternatively, for schemes S2 and S3, the thoracic region connected to the prescribed undeformed elements exhibits excessive expansion in width. The deformations through contraction and expansion at different locations of the model were observed throughout the incremental shape change process.

The highest computational steps are required for the model to reach the targets in deployment scheme S3, followed by S2 and S1. This finding reveals that the cables (or muscles) that are close to and surrounding the monitored nodes, if activated with forced elongations, ease the process of reaching the targets. Although the computational steps increase with the cases with greater target displacement, the increment is not linear.

Axial forces fluctuated within the allowable force limits during the shape change analysis, with a few elements constantly at higher force.

Deployment scheme S1 is more efficient compared to other schemes with lesser computational steps and for the model to preserve the slenderness of the human spine in performing the axial deformation.

This study provides some insights into the different deployment strategies towards cost efficiency while maintaining the stability and self-equilibrium of the bio-tensegrity system during shape change. Understanding the deformation and axial forces of bio-tensegrity during the shape change analysis leads to a better design of the system in terms of solutions to elemental sizes, material properties, control systems etc. The study can be extended to the applications such as deployable structures, mechanical robots or biomechanical studies.

Acknowledgement

This research was funded by Ministry of Higher Education Malaysia, FRGS grant (FRGS/1/2021/TK0/UITM/02/11). In addition, the authors would also like to thank the School of Civil Engineering, College of Engineering, Universiti Teknologi MARA, Shah Alam, Selangor.

Conflicts of Interest

The author(s) declare(s) that there is no conflict of interest regarding the publication of this paper.

References

[1] Bauer, J., Kraus, J. A., Crook, C., Rimoli, J. J., and Valdevit, L. 2021. Tensegrity Metamaterials: Toward Failure-resistant Engineering Systems through Delocalized Deformation. *Advanced Materials*. 33(10): 2005647. https://doi.org/https://doi.org/10.1002/adma.202005647.

[2] Booth, J. W., Cyr-Choiniere, O., Case, J. C., Shah, D., Yuen, M. C., and Kramer-Bottiglio, R. 2021. Surface Actuation and Sensing of a Tensegrity Structure using Robotic Skins. *Soft Robotics*. 8(5): 531-541. https://doi.org/https://doi.org/10.1089/soro.2019.0142.

[3] Busscher, I., Ploegmakers, J. J., Verkerke, G. J., and Veldhuizen, A. G. 2010. Comparative Anatomical Dimensions of the Complete Human and Porcine Spine. *European Spine Journal*. 19: 1104-1114. https://doi.org/http://doi.org/10.1007/s00586-010-1326-9.

[4] Chai Lian, O., Kok Keong, C., Nishimura, T., and Jae-Yeol, K. 2020. Form-finding of Spine Inspired Biotensegrity Model. *Applied Sciences*. 10(18): 6344. https://doi.org/https://doi.org/10.3390/APP10186344.

[5] Chen, B., and Jiang, H. 2022. Instability Results from Purely Rotational Stiffness For General Tensegrity Structure With Rigid Bodies. *Mechanism and Machine Theory*, 167:

104485. https://doi.org/https://doi.org/10.1016/j.mechmachtheory.2021.104485.

[6] Hlavenka, T. M., Christner, V. F. K., and Gregory, D. E. 2017. Neck Posture during Lifting and Its Effect on Trunk Muscle Activation and Lumbar Spine Posture. *Applied Ergonomics*, 62: 28-33. https://doi.org/https://doi.org/10.1016/j.apergo.2017.02.006.

[7] Ingber, D. E., Wang, N., and Stamenović, D. 2014. Tensegrity, Cellular Biophysics, and the Mechanics of Living Systems. *Reports on Progress in Physics*. 77(4): 046603. https://doi.org/http://doi.org/10.1088/0034-4885/77/4/046603.

[8] Levin, S. M. 2002. The Tensegrity-truss as a Model for Spine Mechanics: Biotensegrity. *Journal of Mechanics in Medicine and Biology*. 2(03n04): 375-388. https://doi.org/https://doi.org/10.1142/S0219519402000472.

[9] Liu, Y., Bi, Q., Yue, X., Wu, J., Yang, B., and Li, Y. 2022. A Review on Tensegrity Structures-based Robots. *Mechanism and Machine Theory*. 168: 104571. https://doi.org/https://doi.org/10.1016/j.mechmachtheory.2021.104571.

[10] Oh, C. L., Choong, K. K., and Low, C. Y. 2012. Biotensegrity Inspired Robot–Future Construction Alternative. *Procedia Engineering*. 41: 1079-1084. https://doi.org/https://doi.org/10.1016/j.proeng.2012.07.286.

[11] Oh, C. L., Choong, K. K., Nishimura, T., and Kim, J.-Y. 2022. Multi-Directional Shape Change Analysis of Biotensegrity Model Mimicking Human Spine Curvature. *Applied Sciences*. 12(5): 2377. https://doi.org/https://doi.org/10.3390/app12052377.

[12] Oh, C. L., Choong, K. K., Nishimura, T., Kim, J.-Y., and Hassanshahi, O. 2019. Shape Change Analysis of Tensegrity Models. *Latin American Journal of Solids and Structures*. 16(9): 1-19. https://doi.org/http://dx.doi.org/10.1590/1679-78255407.

[13] Plaut, S. 2023. "Long COVID-19" and Viral "Fibromyalgia-ness": Suggesting a Mechanistic Role for Fascial Myofibroblasts (Nineveh, the shadow is in the fascia). *Frontiers in Medicine*. 10: 952278. https://doi.org/https://doi.org/10.3389/fmed.2023.952278.

[14] Scarr, G. 2012. A Consideration of the Elbow as a tensegrity Structure. *International Journal of Osteopathic Medicine*. 15(2): 53-65. https://doi.org/https://doi.org/10.1016/j.ijosm.2011.11.003.

[15] Swanson, R. L. 2013. Biotensegrity: A Unifying Theory of Biological Architecture with Applications to Osteopathic Practice, Education, and Research—A Review and Analysis. *Journal of Osteopathic Medicine*. 113(1): 34-52. https://doi.org/https://doi.org/10.7556/jaoa.2013.113.1.34.

[16] Wang, Y., Xu, X., and Luo, Y. 2021. Minimal Mass Design of Active Tensegrity Structures. *Engineering Structures*. 234: 111965. https://doi.org/https://doi.org/10.1016/j.engstruct.2021.111965.

[17] Wang, Z., Li, K., He, Q., and Cai, S. 2019. A Light-powered Ultralight Tensegrity Robot with High Deformability and Load Capacity. *Advanced Materials*. 31(7): 1806849. https://doi.org/https://doi.org/10.1002/adma.201806849.

[18] Yang, S., and Sultan, C. 2019. Deployment of Foldable Tensegrity-Membrane Systems via Transition between Tensegrity Configurations and Tensegrity-membrane Configurations. *International Journal of Solids and Structures*. 160: 103-119. https://doi.org/https://doi.org/10.1016/j.ijsolstr.2018.10.017.

[19] Yıldız, K., and Lesieutre, G. A. 2020. Deployment of n-strut Cylindrical Tensegrity Booms. *Journal of Structural Engineering*. 146(11): 04020247. https://doi.org/https://doi.org/10.1061/(ASCE)ST.1943-541X.0002807.

[20] Zappetti, D., Arandes, R., Ajanic, E., and Floreano, D. 2020. Variable-stiffness tensegrity spine. *Smart Materials and Structures*. 29(7): 075013. https://doi.org/https://doi.org/10.1088/1361-665X/ab87e0.

[21] Zhu, D., and Deng, H. 2020. Deployment of Tensegrities Subjected to Load-carrying Stiffness Constraints. *International Journal of Solids and Structures*. 206: 224-235. https://doi.org/https://doi.org/10.1016/j.ijsolstr.2020.08.022.